Discontinuous Dynamic Recrystallization of Inconel 718 Superalloy During the Superplastic Deformation

LINJIE HUANG, FENG QI, PEITAO HUA, LIANXU YU, FENG LIU, WENRU SUN, and ZHUANGQI HU

The superplastic behavior of Inconel 718 superalloy with particular emphasis on the microstructural evolution has been systematically investigated through tensile tests at the strain rate of 10^{-3} s^{-1} and the temperatures ranging from 1223 K to 1253 K (950 °C to 980 °C). Its elongations exceeded 300 pct under all of the experimental conditions and peaked a maximum value of 520 pct at 1223 K (950 °C). Moreover, the stress reached the top value at the strain of 0.3, and then declined until the tensile failure. In addition, we have found that the grain size reduced after deformation while the δ phase precipitation increased. Microstructural evolution during the superplasticity was characterized *via* transmission electron microscope, and the randomly distributed dislocation, dislocation network, dislocation arrays, low-angled subgrains, and high-angled recrystallized new grains were observed in sequence. These new grains were found to nucleate at the triple junction, twin boundary, and near the δ phase. Based on these results, it is deemed that the discontinuous dynamic recrystallization occurred as the main mechanism for the superplastic deformation of Inconel 718 alloy.

DOI: 10.1007/s11661-015-3031-0

I. INTRODUCTION

SUPERPLASTICITY is the ability of a polycrystalline material to exhibit, in generally isotropic manner, very high tensile elongations prior to failure.[1] Due to the low applied force and energy cost, superplastic forming has been widely used to manufacture complex-shaped components in industry. Accordingly, the mechanisms for superplastic deformation have been widely studied and three main models have been proposed.[2–7] (i) Diffusional creep,[6–9] in principle, denotes that high-temperature deformation is a result of the transport of matter by diffusion, rather than dislocation motion.[1] Based on this mechanism, diffusion is induced by a non-hydrostatic stress and atoms flow from compression sites to tension sites. Meanwhile, grain may be elongated along the tensile direction as increasing strain. (ii) Dislocation creep[1,10] refers to the deformation controlled by dislocation slip in the grain lattice. It dominates the superplasticity in some coarse-grained materials, *e.g.*, Class I solid solutions. The slip process involves both glide on slip planes and climb over physical obstacles. (iii) Grain boundary sliding (GBS) accommodation, which is the most popular mechanism for some typical superplastic materials such as aluminum,[11–14] magnesium,[15–18] and titanium[19] alloys are usually accommodation by diffusional transport[3,18] or by dislocation motion[2,4,5] or by a combination of diffusional transport and dislocation motion.[6] One of the common characteristic for the GBS is that the microstructure remains stable during superplastic deformation, *i.e.*, the fine-grain size remains constant. However, there are also some other materials exhibiting complicated microstructural evolution during superplastic deformation, *i.e.*, grain size and shape might be changed, such as nickel-based superalloy Inconel 718(IN718), which may be dominated by another mechanism rather than these three proposed mechanisms.

In order to uncover the mechanism of superplasticity for IN718, microstructural evolution should be clearly understood in the first place. From literature, three main results have been summarized on the microstructural evolution during the superplastic deformation of IN718 alloy. First, the dynamic recrystallization was believed to exist during the process of the superplastic deformation. Ceschini *et al.*[20] studied the superplasticity of IN718 at the temperatures from 1173 K to 1253 K (900 °C to 980 °C) and the dynamic recrystallization was predicted to occur, which was characterized by the presence of a peak point followed by a decreasing flow stress on the true stress–true strain curve. Moreover, a dislocation cell structure suggesting the dynamic recrystallization was observed by Mahoney and Crooks.[21] However, in these investigations, no direct microstructural observation, such as the presence of new recrystallized grain or further analysis on the structural evolution was presented; neither the role of the dynamic recrystallization on the superplasticity was discussed. Second, in contrast, the grain growth was reported with the absence of the dynamic recrystallization.[22–25] Han *et al.*[22] found that IN718 alloy presented good super-

LINJIE HUANG and PEITAO HUA, Ph.D. Students, FENG QI and FENG LIU, Assistant Professors, LIANXU YU, Associate Professor, WENRU SUN, Professor, and ZHUANGQI HU, Professor, Academician, are with the Superalloys Division, Institute of Metal Research, Chinese Academy of Sciences, No.72 Wenhua Road, Shenyang 110016, P.R. China. Contact e-mail: wrsun@imr.ac.cn
Manuscript submitted December 3, 2014.
Article published online July 3, 2015

plasticity when the strain rate and the deformation temperature were varied in the range of 10^{-4} to 10^{-1} s^{-1} and 1213 K to 1293 K (940 °C to 1020 °C). During deformation, the grain size was found to grow slightly from 1213 K to 1253 K (940 °C to 980 °C) while its growth rate was dramatically increased after 1253 K (980 °C). Similar dynamic grain growth was also observed by Lu *et al.*[23] and Qu *et al.*[24] During the superplastic deforming for IN718 in the strain rates of 10^{-3} s^{-1} to 10^{-4} s^{-1} within wide temperature scopes [1193 K to 1253 K (920 °C to 980 °C)], the grain size was found to become larger with the increasing strain.[23] Superplastic elongation >200 pct was reported by Medeiros *et al.*[25] at a high temperature of 1373 K (1100 °C) and strain rate of 10^{-3} s^{-1} while the grain growth was also observed. The dissolving of the precipitated δ phase was proposed to be the reason that led to the grain growth. Third, however, a slight grain size reduction was found by Huang and Blackwell,[26] which is totally different from the second result above. Huang and Blackwell[26] identified the optimum deformation condition for IN718 sheet at 1238 K (965 °C) with a strain rate of 10^{-4} s^{-1} and found a slight grain size reduction. Nevertheless, they believed that the grain reduction was attributed to the increased amount of low-angle boundaries rather than the dynamic recrystallization as there was no direct evidence for the latter. Recently, although the dynamic recrystallization was observed in the hot compression tests of the coarse-grained IN718 alloy,[25,27,28] the strain in the compression is not comparable to the superplastic tensile elongation, meanwhile, the microstructural evolution of the fine-grain IN718 (<10 μm) during superplastic deformation cannot be characterized by the compression tests with the coarse-grain alloy. Therefore, it is controversial that how the grains develop and whether the dynamic recrystallization occurs during the superplastic deformation of IN718 alloy.

IN718 alloy is one of the most widely used nickel-based superalloys in aerospace[29] due to its favorable properties, structural stability, and good corrosion resistance under elevated temperatures, while its superplastic deformation mechanism remains uncertain. Therefore, it is necessary to investigate the superplastic deformation of the alloy. Within this context, the superplastic behavior of IN718 and its microstructure evolution have been systematically investigated. Besides, a possible mechanism responsible for the superplasticity of IN718 alloy, the discontinuous dynamic recrystallization, has been proposed with further discussion.

II. MATERIALS AND EXPERIMENTAL PROCEDURES

A. *Materials*

An IN718 ingot was prepared by vacuum induction melting and vacuum arc remelting and its chemical compositions in weight percent are given as follows: Ni 52.65, Nb 5.20, Mo 3.12, Cr 18.77, Al 0.48, Ti 1.05, C 0.027, P 0.022, B 0.010, Fe balance. The ingot was cogged and hot close-die forged into a cake-like forging after a homogenization treatment. The fine-grained samples used in this paper were cut from the cake-like IN718 forging with an average grain size of 6.9 μm.

B. *Tensile Test*

Superplastic tensile test was carried out on a Shimadzu DCS-25T servo-hydraulic machine at a constant cross-head speed, and the stress–strain curves were drawn from data recorded by the computer under the assumption of volume constancy. Samples were heated in electrical resistance furnace of which the temperature was controlled in three zones with an error less than 3 K (3 °C). Tensile specimens with a gage length of 10 mm and diameter of 5 mm were soaked for 20 minutes at experimental temperatures and then tested to failure at 1223 K, 1238 K, and 1253 K (950 °C, 965 °C, and 980 °C) and the strain rate of 10^{-3} s^{-1}. Because the testing temperature is far above the peak precipitating temperature of δ phase [1173 K (900 °C)], the 20 minutes soaking changed the grain size and the δ phase fraction a little.[30] To retain the deformation microstructure, the specimen was quenched by water as soon as the tensile test was completed.

C. *Microstructure*

The deformed specimens were sectioned parallel to the tensile axis for the microstructure observation *via* scanning electron microscope (SEM) and electron backscatter diffraction (EBSD). The EBSD technique analysis has been widely used to investigate the evolution of microstructure during deformation, the dynamic recrystallization in particular,[31,32] but scarcely it is applied in superplasticity research of the superalloy. In the literature, EBSD was applied on a Hitachi S-3400N scanning electron microscope with a step size of 0.5 μm to study the grain orientation distribution and the grain boundary characteristics of the alloy during the superplastic deformation. The specimens for EBSD were lightly electropolished at 30 V for 15 seconds to produce a strain-free surface and the average indexing rate was close to 90 pct. The calculations of the phase volume fraction and grain sizes were performed in digital image analysis software SISC IAS V8.0 using SEM images. The grain size was measured by using the linear intercept method counting more than 400 grains for each specimen so as to ensure the measurement accuracy. Moreover, to exclude the impact of the difference in the local strain on the microstructural evolution, after failure, the parts with the same final diameter (D = 3 mm) were chosen to analysis the δ phase and the grain size (Table I), where the equal diameter means the equal local strain after failure in different temperatures. In addition, dislocation and recrystallization were examined using transmission electron microscope (TEM) on a JEOL 2010 TEM operated at 200 kV. Thin foils for TEM were prepared by the conventional twin jet polishing techniques using a solution of 10 pct perchloric acid + 90 pct ethyl alcohol (by vol) at 253 K (−20 °C).

Table I. The Average Grain Sizes and δ Phase Fractions of the Specimens Before Deformation and After Tensile Failure at Different Temperatures

Deformation Condition	Undeformed	1223 K (950 °C) 10^{-3} s^{-1}	1238 K (965 °C) 10^{-3} s^{-1}	1253 K (980 °C) 10^{-3} s^{-1}
Average size	6.9 μm	4.2 μm	4.5 μm	5.9 μm
Traverse to stress axis	6.9 μm	3.6 μm	4.1 μm	5.6 μm
Parallel to stress axis	6.9 μm	4.6 μm	5.0 μm	6.1 μm
Grain aspect ratio	1	1.3	1.2	1.1
δ phase fraction	3.7 pct	14.6 pct	5.6 pct	4.1 pct

III. RESULTS

A. *Superplastic Behavior*

Figure 1 compares the specimens before and after tensile failure at 10^{-3} s^{-1} and the temperatures ranging from 1223 K to 1253 K (950 °C to 980 °C). The alloy shows desirable superplastic ductility and the elongation decreased obviously as the temperature increased, which is in agreement with the previous investigations of IN718 alloy.[20,24,33] It is worth noticing that the elongation over 300 pct was obtained at all three temperatures and, in particular, it reaches a maximum elongation of 520 pct at 1223 K (950 °C) and 10^{-3} s^{-1}, which is higher than most of the elongations from previous experiments on IN718 alloy.[26,33,34]

In order to characterize the deformation behavior of the alloy, the stress *vs* strain curves were plotted based on the assumption of uniform deformation. As shown in Figure 2, the flow stress decreased with the increasing temperature, while the curves at 1238 K and 1253 K (965 °C and 980 °C) crossed each other when the strain was over 0.8. In addition, the stress of all of the three curves increased rapidly to the peak values at the strain around 0.3 and then started to decline until failure. Normally, the presence of stress peaks in flow curves suggests the occurrence of dynamic recrystallization.[35]

B. *Grain Size and δ Phase*

Figure 3 illustrates the microstructure before and after superplastic tension. Apparently, in comparison with the undeformed microstructure as shown in Figure 3(a), the grain size of the specimens became smaller and the amount of δ phase increased after tensile failure. In particular, as the deformation temperature raised, the final recrystallized grain size increased while the area fraction of δ phase decreased. It is known that δ phase can effectively pin the grain boundary and limit the grain growth. Here, the decreasing δ phase with the increasing temperature would lead to a corresponding increase in the final grain size. In addition, the δ phase tended to transform into spherical shape and distribute more homogeneously after deformation. Similar phenomenon was observed by Huang and Langdon[36] at 1238 K (965 °C) and 10^{-4} s^{-1}.

More detailed statistics of the grain sizes and the δ phase area fractions are listed in Table I. The grain sizes of all of the three specimens were finer than the undeformed one (d = 6.9 μm), and the grain size increased from 4.2 μm at 1223 K (950 °C) to 5.9 μm at 1253 K (980 °C). Additionally, the grain aspect ratio, which is defined as ratio of grain sizes along longitudinal and transverse directions, was below 1.5 in the deformation condition, which suggests the grains still remain equiaxial relatively after failure. The area fraction of the δ phase grew after deforming at all three temperatures in comparison with the undeformed sample (3.7 pct), indicating the precipitation of δ phase during tension. Meanwhile, a smaller grain size than that of the undeformed specimen was still obtained at the highest temperature 1253 K (980 °C) with the minimum δ phase area fraction, suggesting that the amount of the δ phase 4.1 pct is still effective in pinning the grain boundary to restrict the recrystallized grain growth.

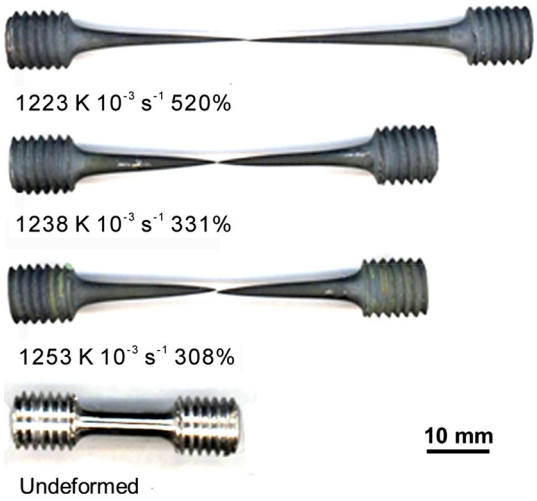

Fig. 1—Tensile specimens of IN718 alloy pulled to failure at 10^{-3} s^{-1} at different temperatures.

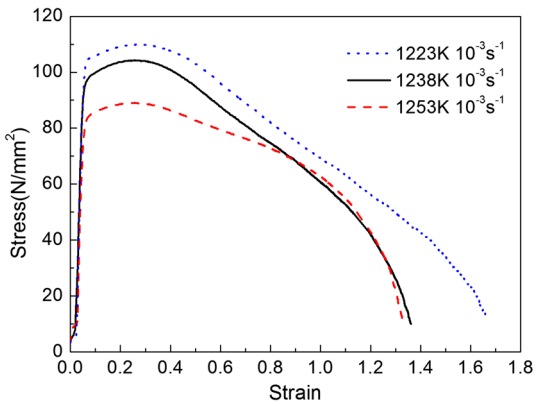

Fig. 2—Variation of stress with strain of the samples deformed at 10^{-3} s^{-1}.

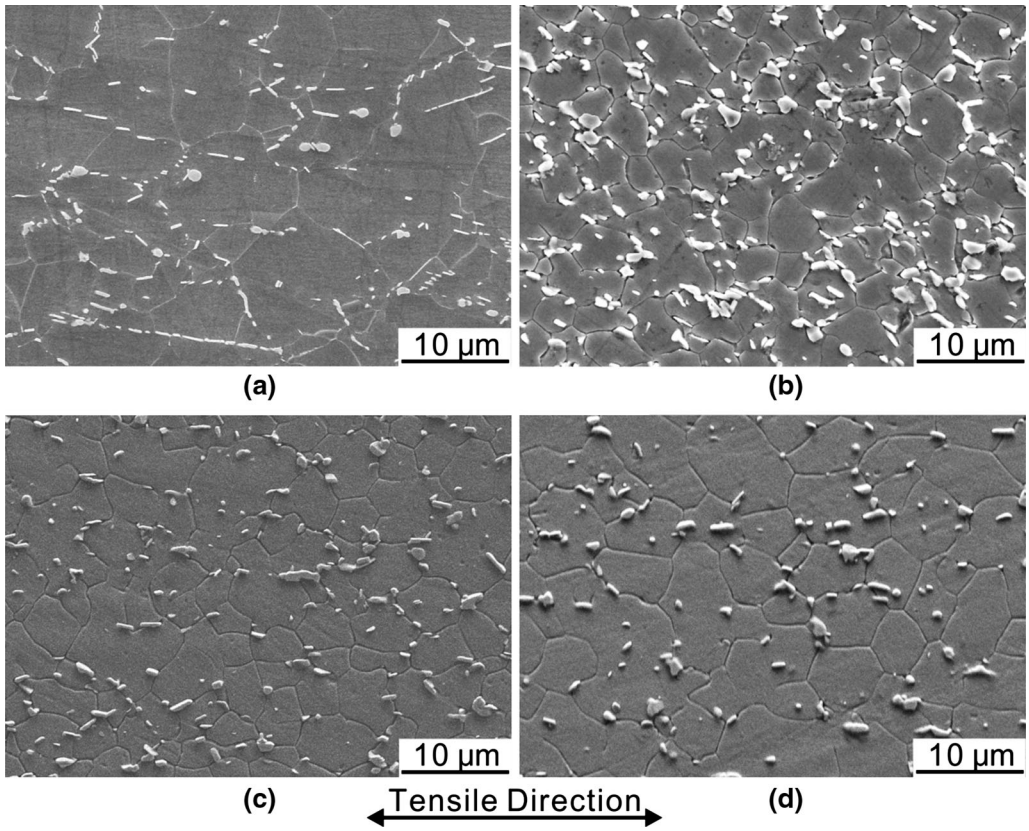

Fig. 3—SEM images taken from the gage section of the specimens before and after tensile failure at 10^{-3} s^{-1} and varied temperatures; (*a*) before tension, (*b*) after failure at 1223 K (950 °C), (*c*) failure at 1238 K (965 °C), and (*d*) failure at 1253 K (980 °C). Note that the δ phase was etched into white to be easily distinguished.

EBSD maps in Figure 4 clearly show the grain morphologies and orientations after failure. Compared with the inverse pole figure inset at the bottom of Figure 4, which helps reveal the color code of the individual grain orientation, no deformation text was found after failure under these experimental conditions, suggesting that full recrystallization happened here.

Therefore, the occurrence of the dynamic recrystallization could be confirmed by a combination of the microstructural details and the variation of stress–strain curve systematically. The growth of the recrystallized grains was restricted by enough δ phases, resulting in finer grains after superplastic deformation.

C. *Dynamic Recrystallization*

In order to further investigate the microstructural evolution during the superplasticity, tensile tests at 1223 K (950 °C) and 10^{-3} s^{-1} were interrupted at the elongation of 50 and 110 pct, and the corresponding backscattered electron images are shown in Figure 5. One can see two types of grain boundary morphologies labeled by A and B. Grain boundaries A were deeply etched, while grain boundaries B were slightly etched, indicating different misorientation angles between Grain boundaries A and B.[37]

Figure 6 compares the microstructures at the elongation of 50 and 110 pct with the undeformed sample through EBSD. The black lines represent the high-angle grain boundaries (HAGBs) above 15 deg, while the green lines represent the low-angle grain boundaries (LAGBs) between 3 and 15 deg. It is worth noting that the undeformed specimen presents few low-angle grain boundaries while the amount of low-angle grain boundaries increased significantly at the elongation of 50 and 110 pct, but decreased to a low proportion at the elongation of 520 pct. The grain size decreased as the elongation increased, reaching the minimum after failure.

The TEM images in Figure 7 illustrate the configuration and development of the dislocation at the elongation of 50 pct. Figure 7(a) shows lots of random dislocation both in the grain and at the grain boundary. The dislocation network and arrays were formed as shown in Figures 7(b) and (c), respectively. From the observation, the dislocation array constituted the main deformation substructures at the elongation of 50 pct, as the subgrain shown in Figure 7(d). In order to better understand the microstructural evolution, the misorientation angles between grains were measured from the deviation of the Kikuchi lines in the diffraction patterns of these grains. In Figure 8(a), the smallest angle with the neighboring grains is 1.9 deg, indicating it is still a subgrain near the δ phase. The selected area diffraction (SAD) pattern of the δ phase in Figure 8(b) indicates the direction of $[10\bar{2}]$of the precipitate. Figure 8(c) shows

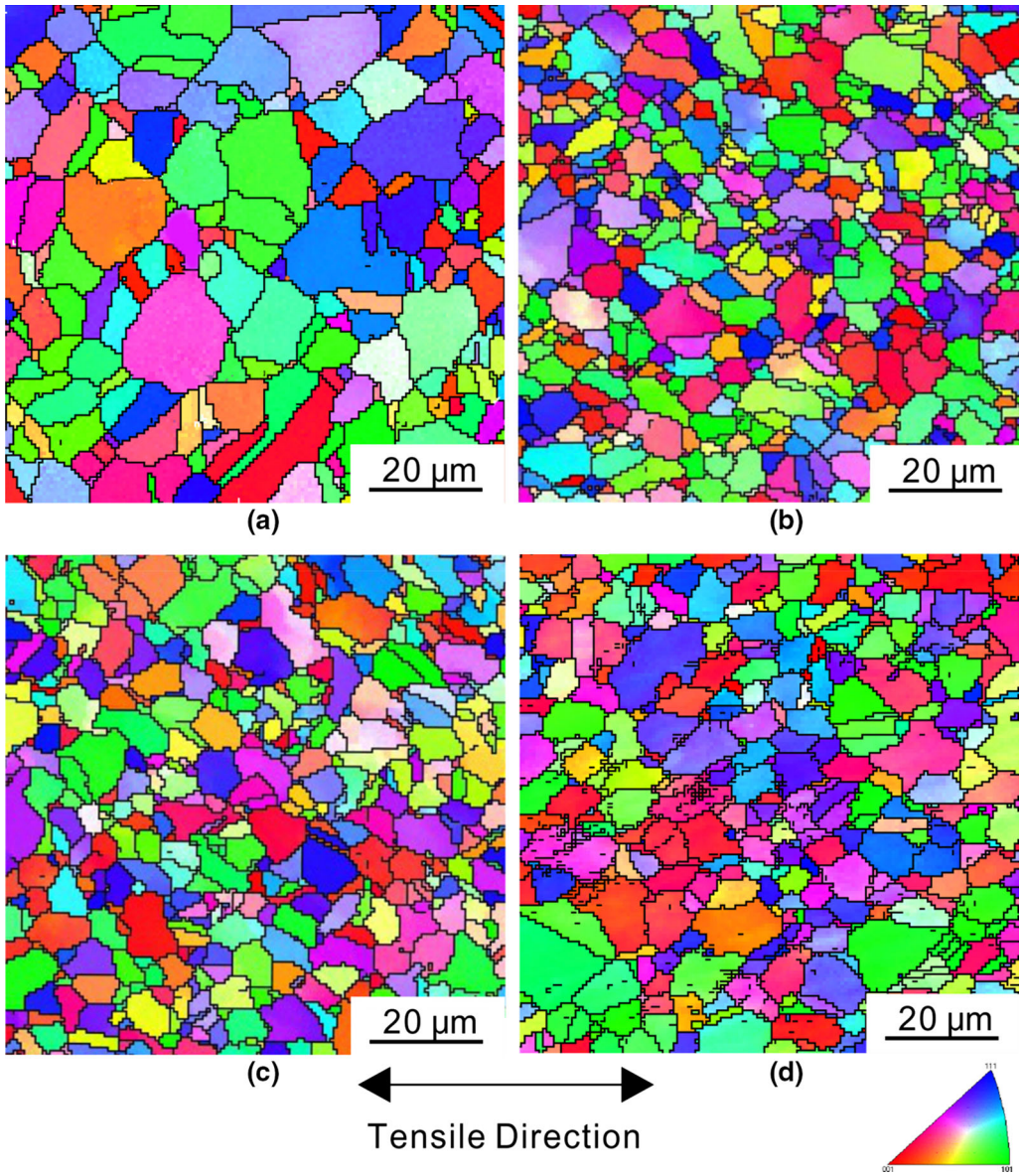

Fig. 4—EBSD micrographs from the gage section of the specimens (*a*) before tension and after tensile failure at 10^{-3} s^{-1} and (*b*) 1223 K (950 °C), (*c*) 1238 K (965 °C), and (*d*) 1253 K (980 °C). The tensile direction and the inverse pole figure were inset.

that the twin boundary can be another important site for the subgrain. The misorientation of the LAGB is 1.6 deg and the twin spots of the SAD pattern in Figure 8(d) were obtained from the direction of [110] of the matrix. It is noticeable that dislocations are moving towards the LAGB of the subgrain to increase the misorientation in Figures 8(a) and (c). Finally, small grains with grain boundary angles larger than 15 deg are observed in Figures 8(e) and (f), indicating they are new recrystallized grains. In addition, it was confirmed that gamma prime or gamma double-prime phase has dissolved and has no impact at the experimental temperatures from the SAD patterns.

From the TEM observation, random dislocations, dislocation network, dislocation arrays, sub-boundaries, and small new recrystallized nucleus presented above are formed in both 50 and 110 pct specimens at all experimental temperatures. Moreover, it is demonstrated that the triple junction, δ phase, and twin boundary are possible recrystallized nucleation sites.

IV. DISCUSSION

A. *Microstructural Characteristics*

The dynamic recrystallization was seldom mentioned in some previous papers,[22–24] while the grain growth was observed to be the primary microstructural characteristic during the deformation, which was promoted by the dissolution of the δ phase with the temperature increasing.[24,33] In this paper, the dynamic recrystallization is confirmed to take place, leading to the refined grain microstructure after tensile failure. The area fractions of the δ phase at all three temperatures are

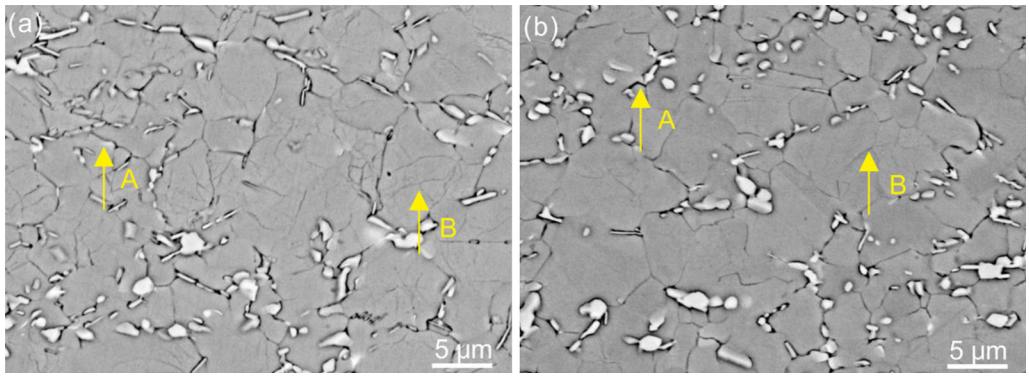

Fig. 5—Backscattered electron micrographs of the specimens tensile tested at 1223 K (950 °C) and 10^{-3} s^{-1}. The tension was interrupted at the elongation of (*a*) 50 pct and (*b*) 110 pct. Grain boundaries A were deeply etched, while grain boundaries B were slightly etched.

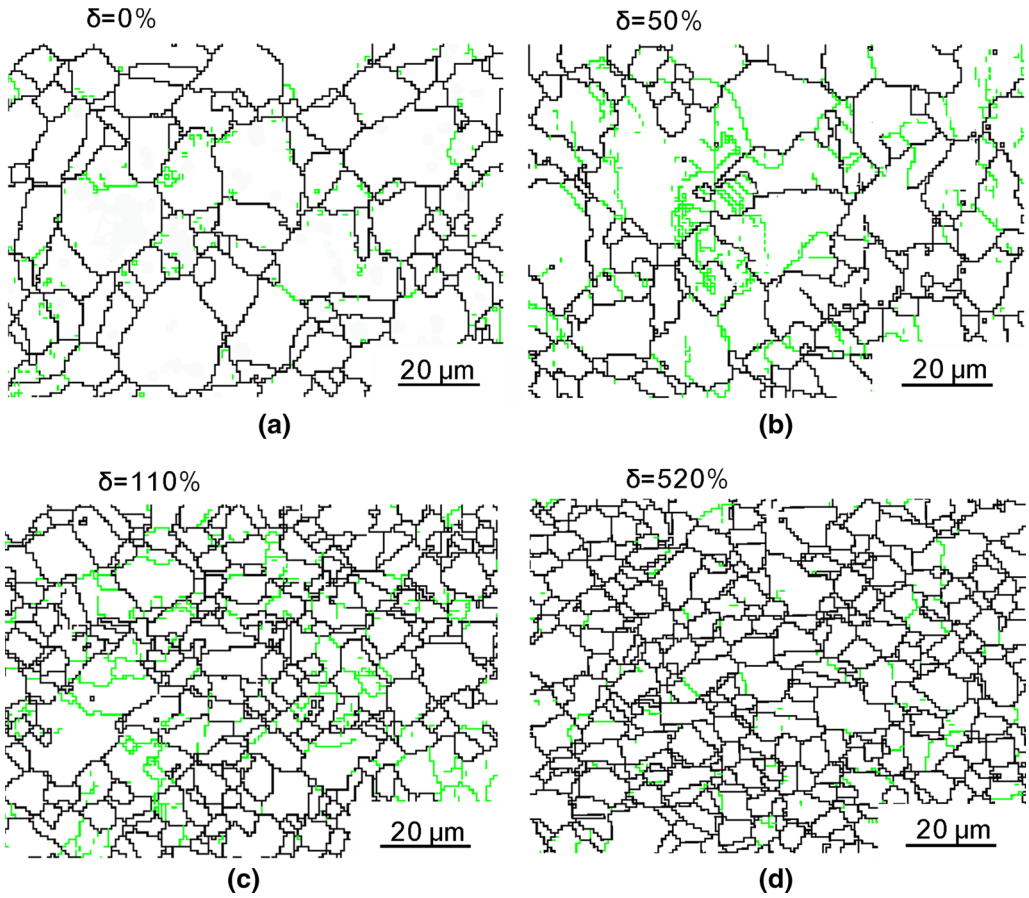

Fig. 6—EBSD images of (*a*) the initial microstructure and tensile tested at 1223 K (950 °C), 10^{-3} s^{-1} after interrupting the tensile test at elongations of (*b*) 50 pct, (*c*) 110 pct, and (*d*) to failure at 520 pct. The green lines represent the low-angle grain boundaries and the black lines stand for the high-angle grain boundaries.

larger than that in the undeformed microstructure. Even though the amount of the δ phase reaches a minimum at 1253 K (980 °C), it is still enough for effectively limiting the grain growth during the superplastic deformation. In addition, it is found that new grain would nucleate near the δ phase (Figure 8(a)), which agrees with the previous result that the δ phase can stimulate the occurrence of dynamic recrystallization.[38] Thus, it is indicated that the lack of δ phase may be responsible for grain growth in those previous investigations.[22–24]

Although the grain size reduction was observed by Huang and Blackwell,[26] it was attributed to the increasing LAGBs, instead of the dynamic recrystallization. It is noteworthy that only the backscattered electron images were used to determine the grain size in their case,[26] making it difficult to distinguish LAGBs

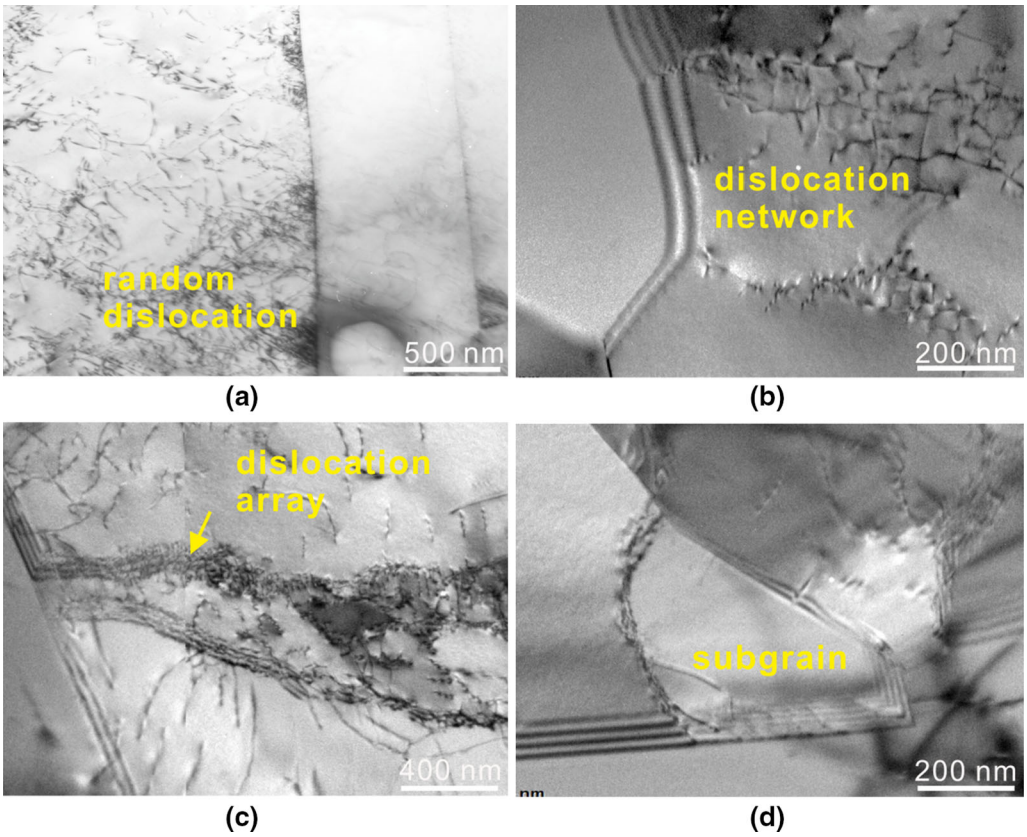

Fig. 7—Typical TEM images of the alloy deformed to 50 pct elongation at 1223 K (950 °C) and 10^{-3} s^{-1}.

and HAGBs exactly. Here the variations of grain size, LAGBs, and HAGBs are clearly demonstrated by using EBSD technique. It is true that some grains are constituted by LAGBs during deformation in Figures 6(b) and (c), but Figure 6(d) obviously illustrates that the final new crystallized grains are mostly formed with HAGBs rather than LAGBs. The EBSD images in Figure 4 can also accurately show the grain size reduction after tension as a result of the dynamic recrystallization.

B. *Mechanism of the Dynamic Recrystallization*

Wang *et al.*[27] investigated the microstructural evolution of IN718 alloy with an average grain size of 176 μm by compression test, and found that the dynamic recrystallization nucleation of the alloy can be operated by bulging of the original grain boundaries, which assists by subgrain rotation or the formation of twinning. It is known that the process of the dynamic recrystallization is closely associated with the generation, motion, and annihilation of dislocation. Specifically, in materials of lower stacking fault energy such as copper, nickel, and stainless steel, the recovery is slow and the dislocation density increases rapidly to the critical value necessary for dynamic recrystallization to occur.[39] As the new grains nucleate, the dislocation will be absorbed or annihilated. Here, the TEM image in Figure 7(a) shows that at the beginning of superplastic deformation, the dense dislocations are predominant in the microstructure and the dislocation network can be observed in Figure 7(b). As the strain increases, dislocations move into dislocation arrays by climbing or slipping (Figure 7(c)). With further deforming, the dislocation arrays absorb more dislocations and transform into sub-boundary (Figure 7(d)). The misorientation between two neighbor subgrains enlarges as the sub-boundaries absorb the dislocations, resulting in the occurrence of the LAGB (1.9 deg in Figure 8(a) and 1.6 deg in Figure 8(c)). With a large amount of dislocations keep moving towards the LAGB to increase its misorientation, LAGB transforms into HAGB after its misorientation exceeds 15 deg. Finally, new crystallized grains are formed by the HAGBs in Figures 8(e) and (f). Figure 6 also shows the amount variation of LAGBs and HAGBs.

The occurrence of the dynamic recrystallization was once denied,[26] because the process, in which low-angle boundaries are progressively transformed into high-angle (disordered) boundaries through the absorption of dislocation, was not proven. In this investigation, the dynamic recrystallization process was clearly demonstrated, which released deforming energy and made superplastic deforming feasible by overcoming the strain hardening. Similar dynamic recrystallization process was found in some intermetallics, *i.e.*, NiAl polycrystals.[40] However, apart from the alloy system, the initial grain size and the recrystallization mechanism are different from this experiment.

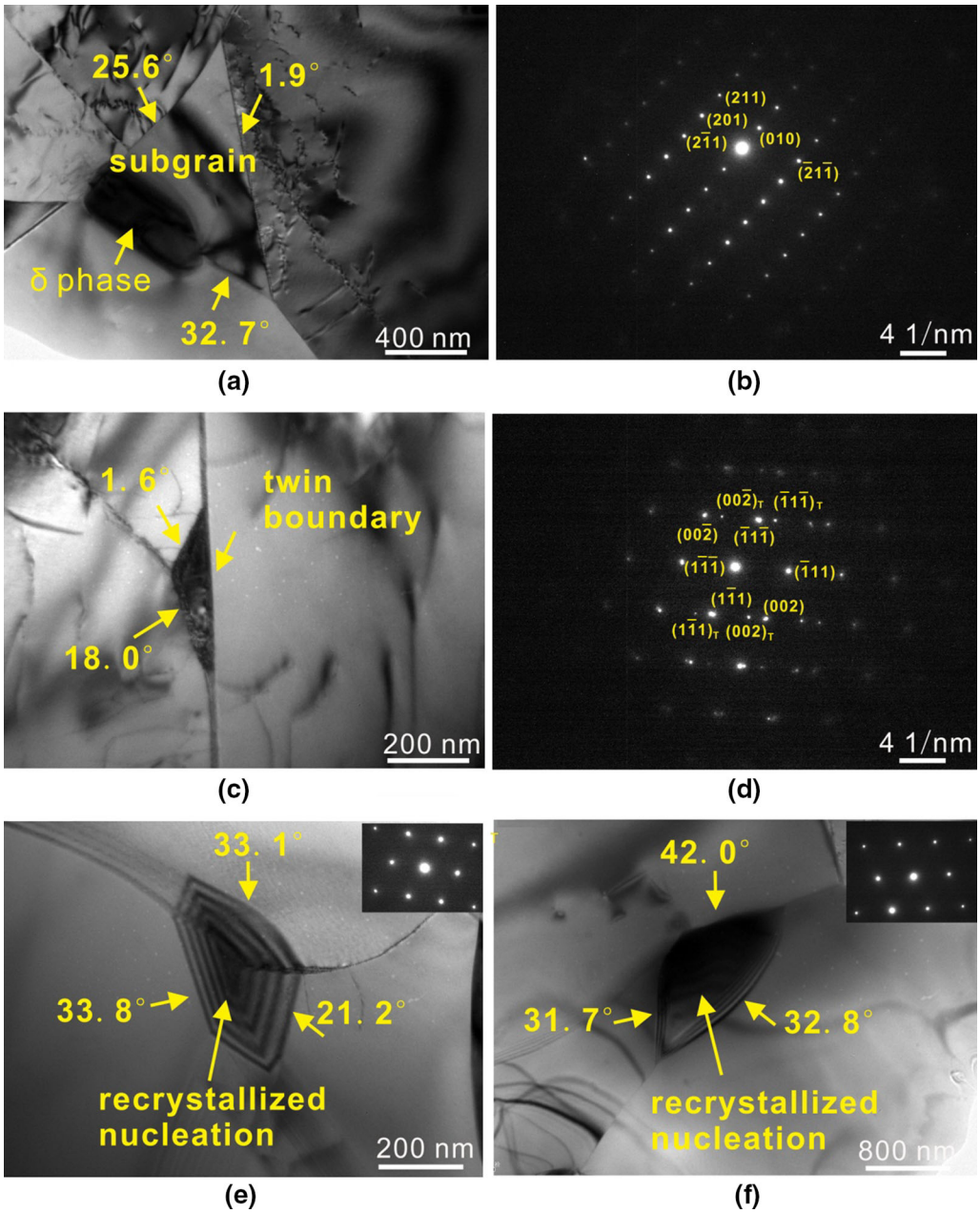

Fig. 8—Typical TEM images of the alloy deformed to 110 pct elongation at 1223 K (950 °C) and 10^{-3} s^{-1}, (*a*) a subgrain near the δ phase; (*b*) the δ phase SAD pattern from [10$\bar{2}$]; (*c*) a subgrain near the twin boundary; (*d*) the twin SAD pattern from [110]; (*e*) and (*f*) the recrystallization nucleation with the misorientations labeled and the corresponding SAD pattern from [110] inset.

Dynamic recrystallization can be classified into either continuous or discontinuous dynamic recrystallization. On the one hand, during the continuous recrystallization, dislocations remain in the recrystallized grains and dislocation substructures develop homogeneously without nucleation of new grains, which do not agree with the observation in Figure 8, where the new grains are observed to nucleate in the triple junction, twin boundary, and near the δ phase. On the other hand, the discontinuous recrystallization removes dislocations through the sweeping action of high-angle boundaries, and substructures vary from grain to grain and develop inhomogeneously.[41,42] When the discontinuous recrystallization occurs, there is a relatively sharp change in the proportion of HAGB or LAGB as the deformed substructure is consumed by the recrystallizing grains.[39] Moreover, discontinuous recrystallization will experience nucleation and growth process. In this experiment, the proportion change of LAGB (Figure 6) and the new grain nucleation (Figure 8) are observed. These experimental results agree well with the typical characteristics of the discontinuous recrystallization. Therefore, it can be confirmed that the dynamic recrystallization happens during the superplastic deformation of IN718 is discontinuous.

As can be confirmed, the dynamic recrystallization happens during the superplastic deformation of IN718 is discontinuous.

C. *Role of the Dynamic Recrystallization in the Superplastic Deformation*

GBS, as one of the most popular mechanisms in conventional fine-grained superplastic deformation, often requires that the grain size keeps nearly constant and the grain boundaries between adjacent matrix grains maintain high energy (high angles and disordered) during the superplasticity.[3–7] Usually, GBS is experimentally demonstrated by the offset of scratch lines on a sample surface after test.[1] However, in this study, the grain size became smaller without any direct evidence associated with GBS. Furthermore, Figure 6 shows a number of LAGBs during deformation, which are low-energy grain boundaries and do not readily slide during superplastic deforming.[1] In addition, the distribution of δ phase along the grain boundary would strongly restrict the GBS during the deformation. All these facts suggest GBS may not be the dominant deformation mechanism for the alloy.

In terms of the diffusional creep, the elongation is supposed to increase with the elevating temperature as the atom diffusion rate increases. In addition, the grain will be elongated parallel to stress direction with increasing strain.[1] However, in our experiment, the superplastic elongation decreases from 1223 K to 1253 K (950 °C to 980 °C), and the grains after failure remain equiaxed (Table I) without deformation text (Figure 4), suggesting the diffusional creep plays a limited role during deformation.

In the dislocation creep mode, the overall creep rate is controlled by the slower process of dislocation glide and climb rates. In the alloys with low or intermediate stacking fault energy, *e.g.*, nickel, the glide proceeds slowly.[39] Here, the dislocation motion and tangling are energy storing process for the dynamic recrystallization.

In this paper, the discontinuous dynamic recrystallization has been confirmed as the main mechanism for the superplasticity of the alloy according to three factors: (i) the deformation parameter; the deformation temperatures are above the temperature of dynamic recrystallization 1123 K (850 °C)[43]; (ii) alloy factor; in the alloys with low or intermediate stacking fault energy, *e.g.*, nickel or stainless steel, the dynamic recovery proceeds slowly while the high dislocation density stimulates the occurrence of dynamic recrystallization;[44] and (iii) more importantly, the microstructural characteristics: fine grains with a large amount of grain boundaries and δ phase, which provide nucleation sites for recrystallization.[45] Meanwhile, the δ phase can effectively restrict the growth of recrystallized grains.

During the discontinuous dynamic recrystallization of the superplastic deformation, both the dislocation motion and the recrystallization contribute much to the ductility. Han *et al.*[22] found lots of dislocations tangled near the precipitate phase and believed that the deformation mechanism of IN718 is based on dislocation proliferation and movement. The present observation about dislocation suggests that the dislocation motion, including climbing, gliding, and array formation, plays an important role during the superplastic deformation, which is different from the superplastic deformation of those conventional alloy, such as aluminum and titanium alloys,[1,4] where dislocation is scarcely found. As the dynamic recrystallization during the superplasticity of IN718 alloy is discontinuous, a critical number of dislocations are required to store enough strain energy for the formation of new grain. The fact indicates the dynamic recrystallization is a dislocation-induced process.

In the dynamic recrystallization induced by dislocation, the dislocation motion influences the deformation in two aspects. On one hand, the dislocation slip contributes to the ductility and stores the energy of deformation as in the conventional deformation. On the other hand, the tangled dislocations lead to strain hardening, which limit further deformation. According to the laws of recrystallization,[39] the driving force of the nucleation and growth in recrystallization is provided by the stored energy of deformation. In other words, the stored energy is consumed by dynamic recrystallization. As a result, the strain hardening was balanced by the annihilation of the dislocations and the dynamic recrystallization, making the deformation continues. As the superplastic deformation moves on, new dislocation forms, slips, tangles, and finally leads to another period of dynamic recrystallization. In the next dislocation-induced dynamic recrystallization process, the dislocation and recrystallization interact in the way discussed above. Therefore, it is believed that the superplastic deformation of IN718 superalloy is dominated by the dislocation-induced discontinuous dynamic recrystallization.

The discontinuous dynamic recrystallization makes the superplastic deformation not only a manufacturing method but also a grain-refined process for IN718 alloy, which enhances the strength and the low-cycle fatigue property of the final structure, and can save the fabricating cost in practical production.

V. CONCLUSIONS

The superplastic tensile tests were conducted on IN718 superalloy to investigate its superplastic behavior and uncover its deformation mechanism at the strain rate of 10^{-3} s^{-1} and temperatures ranging from 1223 K to 1253 K (950 °C to 980 °C). The conclusions can be summarized as follows:

1. IN718 alloy exhibits desirable superplastic ductility, achieving elongation exceeding 300 pct under all the tensile conditions and peaking a maximum value of 520 pct at 1223 K (950 °C).
2. The grain size of the fractured specimen is smaller than that of the undeformed specimen, and the δ phase precipitation is increased by the superplastic deformation. In addition, the final grain size is increased while the δ phase precipitation is decreased with the elevating experimental temperature.

3. It is proved that the discontinuous dynamic recrystallization is the main mechanism for the superplastic deformation of IN718 alloy based on the facts of the grain refinement and the microstructure evolution from randomly distributed dislocation, dislocation network, and dislocation array, to low-angled subgrains and high-angled recrystallized fresh grains.

REFERENCES

1. T.G. Nieh, J. Wadsworth, and O.D. Sherby: *Superplasticity in Metals and Ceramics*, Cambridge University Press, New York, 2005, p. 1.
2. R.C. Gifkins: *Metall. Trans. A*, 1976, vol. 7A, pp. 1225–32.
3. M.F. Ashby and R.A. Verrall: *Acta Metall.*, 1976, vol. 21, pp. 149–63.
4. A. Ball and M.M. Hutchison: *Mater. Sci. Technol.*, 1969, vol. 3, pp. 1–7.
5. A.K. Mukherjee: *Mater. Sci. Eng.*, 1971, vol. 8, pp. 83–89.
6. J.R. Spingarn and W.D. Nixa: *Acta Metall.*, 1978, vol. 26, pp. 1389–98.
7. R.L. Coble: *J. Appl. Phys.*, 1963, vol. 34, pp. 1679–82.
8. W.J. Kim and I.B. Park: *Scripta Mater.*, 2013, vol. 68, pp. 179–82.
9. T. Lee, Y. Park, and W. Kim: *Mater. Sci. Eng. A*, 2013, vol. 580, pp. 133–41.
10. O. Sherby and J. Weertman: *Acta Metall.*, 1979, vol. 27, pp. 387–400.
11. A. Alhamidi and Z. Horita: *Mater. Sci. Eng. A*, 2015, vol. 622, pp. 139–45.
12. Z.Y. Ma, F.C. Liu, and R.S. Mishra: *Acta Mater.*, 2010, vol. 58, pp. 4693–4704.
13. G. Rai and N.J. Grant: *Metall. Trans. A*, 1983, vol. 14A, pp. 1451–58.
14. J.H. Han and F.A. Mohamed: *Metall. Mater. Trans. A*, 2011, vol. 42A, pp. 3969–78.
15. A. Mohan, W. Yuan, and R.S. Mishra: *Mater. Sci. Eng. A*, 2013, vol. 562, pp. 69–76.
16. W.J. Kim, S.W. Chung, C.S. Chung, and D. Kum: *Acta Mater.*, 2001, vol. 49, pp. 3337–45.
17. R. Panicker, A.H. Chokshi, R.K. Mishra, R. Verma, and P.E. Krajewski: *Acta Mater.*, 2009, vol. 57, pp. 3683–93.
18. Y. Wang and J. Huang: *Metall. Mater. Trans. A*, 2004, vol. 35A, pp. 555–62.
19. X.J. Zhu, M.J. Tan, and W. Zhou: *Scripta Mater.*, 2005, vol. 52, pp. 651–55.
20. L. Ceschini, G.P. Cammarota, G.L. Garagnani, F. Persiani, and A. Afrikatnov: *Mater. Sci. Forum.*, 1994, vols. 170–172, pp. 351–58.
21. M.W. Mahoney and R. Crooks: *Superplasticity in Aerospace*, The Metallurgical Society, Phoenix, 1988, pp. 331–44.
22. X. Han, L. Wu, H. Xia, R. Liu, S. Wang, and Z. Chen: *J. Mater. Process. Technol.*, 2003, vol. 137, pp. 17–20.
23. H.J. Lu, X.C. Jia, K.F. Zhang, and C.G. Yao: *Mater. Sci. Eng. A*, 2002, vol. 326, pp. 382–85.
24. F.S. Qu, Z. Lu, F. Xing, and K.F. Zhang: *Mater. Des.*, 2012, vol. 39, pp. 151–61.
25. S. Medeiros, Y. Prasad, W.G. Frazier, and R. Srinivasan: *Mater. Sci. Eng. A*, 2000, vol. 293, pp. 198–207.
26. Y. Huang and P.L. Blackwell: *Mater. Sci. Technol.*, 2003, vol. 19, pp. 461–66.
27. Y. Wang, W.Z. Shao, L. Zhen, and X.M. Zhang: *Mater. Sci. Eng. A*, 2008, vol. 486, pp. 321–32.
28. F.-L. Sui, L.-X. Xu, L.-Q. Chen, and X.-H. Liu: *J. Mater. Process. Technol.*, 2011, vol. 211, pp. 433–40.
29. R.C. Reed: *The Superalloys, Fundamentals and Applications*, Cambridge University Press, Cambridge, 2006, pp. 1–2.
30. S. Azadian, L.-Y. Wei, and R. Warren: *Mater. Charact.*, 2003, vol. 53, pp. 7–16.
31. D. Jorge-Badiola, A. Iza-Mendia, and I. Gutiérrea: *J. Microscopy*, 2007, vol. 228, pp. 373–83.
32. A.K. Mukhopadhyay, A. Kumar, S. Raveendra, and I. Samajdar: *Scripta Mater.*, 2011, vol. 64, pp. 386–89.
33. H.J. Lv, C. Yao, X. Jia, and K. Zhang: *Chin. J. Mech. Eng.*, 2003, vol. 16, pp. 72–74.
34. M. Urdanpilleta, J.M. Martinez-Esnaola, and J.G. Sevillano: *Mater. Trans. A*, 2005, vol. 46, pp. 1711–19.
35. W.-Y. Kim, S. Hanada, and T. Takasugi: *Acta Mater.*, 1997, vol. 46, pp. 3593–3604.
36. Y. Huang and T.G. Langdon: *J. Mater. Sci.*, 2007, vol. 42, pp. 421–27.
37. D. Jiang and D. Lin: *Mater. Lett.*, 2002, vol. 57, pp. 747–52.
38. Y. Wang, L. Zhen, W. Shao, L. Yang, and X. Zhang: *J. Alloys Compd.*, 2009, vol. 474, pp. 341–46.
39. F.J. Humphreys and M. Hatherly: *Recrystallization and Related Annealing Phenomena*, 2nd ed., Elsevier, Oxford, 2004, p. 485.
40. X. Du and B. Wu: *Metall. Mater. Trans. A*, 2005, vol. 36A, pp. 3343–51.
41. J.C. Tan and M.J. Tan: *Mater. Sci. Eng. A*, 2003, vol. 339, pp. 81–89.
42. T. Sakai, A. Belyakov, R. Kaibyshev, H. Miura, and J. Jonas: *Prog. Mater. Sci.*, 2014, vol. 60, pp. 130–207.
43. E. Loria: *Superalloys 718, 625, 706 and Various Derivatives*, TMS, Pennsylvania, 1994, p. 303.
44. H. Yuan and W.C. Liu: *Mater. Sci. Eng. A*, 2005, vol. 408, pp. 281–89.
45. S.-H. Zhang, H.-Y. Zhang, and M. Cheng: *Mater. Sci. Eng. A*, 2011, vol. 528, pp. 6253–58.